NEOPLASIA
www.neoplasia.com

Volume 10 Number 4 April 2008 pp. 347–353 347

Utility of a Herpes Oncolytic Virus for the Detection of Neural Invasion By Cancer[1]

Ziv Gil*, Kaitlyn J. Kelly*, Peter Brader*†, Jatin P. Shah*, Yuman Fong* and Richard J. Wong*

*Department of Surgery, Memorial Sloan-Kettering Cancer Center, New York, NY 10021, USA; †Department of Radiology, Memorial Sloan-Kettering Cancer Center, New York, NY 10021, USA

Abstract

Prostate, pancreatic, and head and neck carcinomas have a high propensity to invade nerves. Surgical resection is a treatment modality for these patients, but it may incur significant deficits. The development of an imaging method able to detect neural invasion (NI) by cancer cells may guide surgical resection and facilitate preservation of normal nerves. We describe an imaging method for the detection of NI using a herpes simplex virus, NV1066, carrying tyrosine kinase and enhanced green fluorescent protein (eGFP). Infection of pancreatic (MiaPaCa2), prostate (PC3 and DU145), and adenoid cystic carcinoma (ACC3) cell lines with NV1066 induced a high expression of eGFP *in vitro*. An *in vivo* murine model of NI was established by implanting tumors into the sciatic nerves of nude mice. Nerves were then injected with NV1066, and infection was confirmed by polymerase chain reaction. Positron emission tomography with [^{18}F]-2′-fluoro-2′-deoxyarabinofuranosyl-5-ethyluracil performed showed significantly higher uptake in NI than in control animals. Intraoperative fluorescent stereoscopic imaging revealed eGFP signal in NI treated with NV1066. These findings show that NV1066 may be an imaging method to enhance the detection of nerves infiltrated by cancer cells. This method may improve the diagnosis and treatment of patients with neurotrophic cancers by reducing injury to normal nerves and facilitating identification of infiltrated nerves requiring resection.

Neoplasia (2008) 10, 347–353

Introduction

Prostate, pancreatic, and head and neck carcinomas are among the leading causes of cancer death in the United States. These tumors are also notorious for their ability to invade nerves. More than 85% of patients with pancreatic and prostate carcinomas and 60% of those with adenoid cystic carcinomas present with neural invasion (NI) at the time of diagnosis [1,2]. One of the main treatment modalities available for these patients is surgical resection of the primary tumor along with regional nerves suspected of being infiltrated by cancer [3]. Unfortunately, such treatment often causes major morbidity and impaired quality of life due to loss of nerve function. Erectile dysfunction, urinary incontinence, facial numbness, facial paralysis, hoarseness, dysphagia, and dysarthria are a few examples of the morbidity associated with neural injury as a consequence of radical tumor resection [4]. For this reason, some patients are willing to compromise survival outcomes in exchange for improved function when choosing therapy [5].

The decision to resect or preserve nerves in close proximity to the tumor is often made intraoperatively. Because preoperative imaging modalities have a limited ability to identify NI by cancers, the parameters currently available for surgeons to determine if a nerve is invaded by cancer include preoperative neurologic symptoms, tumor adherence to nerves, and evidence of gross neural infiltration during surgery [6]. Because of limitations in the ability to accurately identify NI by cancers, normal nerves may sometimes be resected, needlessly inflicting the morbidity of lost nerve function. Conversely, the consequences of not resecting a nerve infiltrated by cancer include higher rates of disease

Abbreviations: HSV, herpes simplex virus; PET, positron emission tomography; eGFP, enhanced green fluorescent proteins; NI, neural invasion; [^{18}F]-FEAU, [^{18}F]-2′-fluoro-2′-deoxyarabinofuranosyl-5-ethyluracil; PFU, plaque-forming unit; MOI, multiplication of infection; cDNA, complementary DNA; PCR, polymerase chain reaction

Address all correspondence to: Richard J. Wong, Head and Neck Service, C-1069, Department of Surgery, Memorial Sloan-Kettering Cancer Center, 1275 York Avenue, New York, NY 10065. E-mail: wongr@mskcc.org

[1]Supported by grants from the American Head and Neck Society, the American College of Surgeons and the Flight Attendant Medical Research Institute (R. J. W.). Supported in part by the National Institutes of Health grants R25-CA096945-3 (P. B.), RO1 CA75416 (Y. F.), and from the Israeli Association of Otolaryngology Head and Neck Surgery (Z. G.).

Received 24 November 2007; Revised 24 November 2007; Accepted 15 January 2008

DOI 10.1593/neo.07981

recurrence and reduced survival [7]. An imaging method to accurately detect the presence of NI by cancer would be of significant value to the surgeon facing this intraoperative dilemma.

Current imaging techniques for the detection of cancer dissemination along nerves are limited and can only detect gross tumor infiltration. There is currently no effective imaging modality to reliably identify the presence and extent of NI by cancer [8]. A surgeon might consider intraoperative biopsies and frozen-section pathology assessment from sites of suspected nerve infiltration. However, this technique itself may cause unnecessary nerve injury.

Oncolytic herpes simplex viruses (HSVs) are replication-competent vectors that can selectively infect cancer sells. These viruses can replicate within cancer cells and induce expression of specific transgenes coded by the viral genome [9]. Previous studies have shown that HSVs carrying the transgene for enhanced green fluorescent protein (eGFP) can be used to image tumors by fluorescence microscopy [10]. Our goal was to develop a reliable imaging method for the assessment of NI by cancer using herpes vectors. Such a system may potentially allow surgeons to identify and selectively target resection of nerves infiltrated by cancer, preventing unnecessary neural injury to nerves not involved by cancer.

The ability of an NV1066-based imaging to identify NI by prostate, pancreatic, and head and neck carcinomas was assessed in this study. Our results demonstrate that NV1066 can be used as a safe and effective imaging method allowing for the detection of nerves infiltrated by cancer, both in a preoperative and intraoperative setting.

Materials and Methods

Cell Lines

The human pancreatic adenocarcinoma cell line MiaPaCa2, the prostate cell lines PC3 and DU145, and the adenoid cystic carcinoma cell line ACC3 were used. Cells were grown in F12K medium adjusted to contain 1.5 g/l sodium bicarbonate (PC3), in high-glucose Dulbecco's modified Eagle's medium (MiaPaCa2 and DU145) and in Roswell Park Memorial Institute (RPMI)-1640 medium (ACC3). All media contained 10% fetal calf serum, penicillin, and streptomycin. Cells were maintained in 5% CO_2 in a 37°C humidified incubator.

Viruses

NV1066 is an oncolytic HSV whose construction was previously described [10]. In brief, it is a replication-competent, attenuated herpes simplex type-1 viral strain (F′ strain) that expresses eGFP on infection of cancer cells. The transgene for eGFP is inserted into the deleted internal repeat sequence region under the control of a cytomegalovirus promoter. NV1066 is also deficient in the UL23 sequence, the internal repeat sequence containing single copies of the viral genes *ICP-4*, *ICP-0*, and $\gamma_1 34.5$. These genomic deletions decrease viral virulence and enhance tumor specificity. Viruses were propagated on Vero cells and titered by standard plaque assay. NV1066 was provided by Medigene, Inc. (San Diego, CA).

In Vitro *Model of NI*

Mice (Balb/c, 4–6 weeks old) were anesthetized, and their dorsal root ganglia (DRG) was implanted ~500 μm adjacent to a colony of carcinoma cells in growth factor–depleted Matrigel matrix (BD Biosciences, Bedford, MA). Cultures were grown in media containing 10% fetal calf serum at 37°C and 5% CO_2. NV1066 was injected into the Matrigel in an area between the cancer colony and the DRG, 1 to 4 days before imaging.

In Vivo *Model of NI*

Six-week-old athymic nude mice (National Cancer Institute, Bethesda, MD) were anesthetized with inhalational isoflurane for all procedures. The left sciatic nerve was then exposed deep to the femorococcygeus and biceps femoris muscles. Human carcinoma cells were microscopically injected into the perineurium of the sciatic nerve, distal to the bifurcation of the tibial and common peroneal nerves. Slow microinjection of 3 μl of cell suspension at a concentration of 1×10^5 cell/μl was performed using a 10-μl Hamilton syringe over a 2-minute period. Seven days after establishment of intraneural tumors, 5×10^7 viral plaque-forming units (PFUs) of NV1066 or saline were injected into the sciatic nerve. In some experiments, NV1066 was injected into nerves without tumors. For histologic analysis, mice were euthanized 48 hours after viral infection, the sciatic nerve excised, frozen in Tissue Tek (Sakura Finetek, Torrance, CA) solution, and cut into 8-μm-thick sections. Other groups were observed for up to 7 weeks for assessment of tumor response, nerve function, or signs of morbidity.

Measures of Sciatic Nerve Function

Sciatic nerve function was measured weekly. The sciatic nerve innervates the hind limb paw muscles. Functional measures for monitoring tumor NI included: (1) Gross behavior — signs of motor weakness or repetitive biting of the hind limb were monitored for 10 minutes once a week; and (2) Limb function — graded according to hind limb paw response to manual extension of the body, with scores ranging from 4 = normal to 1 = total paw paralysis.

Fluorescence Imaging

NV1066-infected cancer cells were imaged *in vitro* by fluorescence microscopy. Cancer cells (5×10^4) were plated in four-well chamber slides (Laboratory-Tek, San Diego, CA). After overnight incubation at 37°C, cells were infected with NV1066 at a multiplication of infection (MOI; the ratio of PFU to tumor cells) of 0.1 to 10. Cells treated with phosphate-buffered saline served as controls. The cells were examined at different time intervals using a microscope (Axiovert 400; Carl Zeiss, Oberkochen, Germany). The MetaMorph System (Universal Imaging, Downingtown, PA) was used for image analysis and eGFP quantification. Cells were examined under a bright field microscope with a 4′,6-diamidino-2-phenylindole fluorescence filter to assess cellular and nuclear morphology and viability.

In vivo imaging was performed in both bright field and fluorescence modes using a stereomicroscope (Olympus America, Melville, NY). The excitation filter was fixed-passage through a 470 ± 40-nm wavelength light because eGFP has a minor excitation peak at 475 nm. The emission filter was fixed at 500 nm to accommodate the emission peak of eGFP at 509 nm. The image-capture system consisted of a digital CCD camera (Retiga EX; Qimaging, Burnaby, Canada).

[^{18}F]-FEAU Production

[^{18}F]-FEAU (2′-fluoro-2′-deoxyarabinofuranosyl-5-ethyluracil) was synthesized by coupling the radiolabeled fluoro sugar with the silylated pyrimidine derivative following a procedure previously reported by Serganova et al. [11]. The specific activity of the product was ~37 GBq/μmol (~1 Ci/μmol); radiochemical purity was >95% following purification by HPLC.

Positron Emission Tomography

Animals were intravenously injected with ~250 μCi (9.25 MBq) of [^{18}F]-FEAU tracer 2 hours before positron emission tomography (PET) imaging. Mice were anesthetized with 2% isoflurane, degutted, and imaged with a dedicated small-animal PET scanner (Focus 120 micro-PET; Concorde Microsystems, Knoxville, TN) [12]. Images were acquired using a transaxial field-of-view of 10 cm and an axial field-of-view of 7.8 cm. An energy window of 350 to 750 keV and a coincidence timing window of 6 nanoseconds were used. The resulting list-mode data were sorted into two-dimensional histograms by Fourier rebinning, and transverse images were reconstructed by filtered backprojection into a 128 × 128 × 63 (0.72 × 0.72 × 1.3 mm^3) matrix. Image analysis was performed using the ASIPro software (Concorde Microsystems). After imaging, the specimens were excised, weighed, and measured for radioactivity using a gamma counter (Packard United Technologies, Downers Grove, IL). The radioactivity is expressed as the percentage of radiotracer-injected dose per gram of tissue (%[ID/g]). Animals were sacrificed by CO_2 inhalation.

Quantitative Reverse Transcription–Polymerase Chain Reaction

Sciatic nerves of athymic nude mice were injected with NV1066 at 5 × 10^7 PFU or with saline for control animals. At 48 hours after injection, mice were euthanized by CO_2 inhalation. Brain, spinal cord, and sciatic nerve tissues were excised and homogenized separately in 1.2-ml TRIzol reagent (Invitrogen, Carlsbad, CA). After the addition of chloroform, samples were centrifuged for phase separation. RNA was precipitated from the aqueous phase with isopropanol and treated with DNase (DNA-*free*; Ambion, Austin, TX) according to the manufacturer's directions. Complementary DNA (cDNA) was reverse-transcribed from tissue RNA using random hexamer priming. For each sample, 250 to 500 ng of total RNA was added to 4 μl of 5× RT buffer (Invitrogen), 10 pmol random hexamers, 12.5 μmol each of 2′-deoxyadenosine 5′-triphosphate, 2′-deoxythymidine 5′-triphosphate, 2′-deoxyguanosine 5′-triphosphate, and 2′-deoxycytidine 5′-triphosphate, 200 U of reverse transcriptase (Invitrogen), and 20 U of RNasin (Promega, Madison, WI), bringing the total volume to 20 μl. Quantitative reverse transcription–polymerase chain reaction (RT-PCR) was performed on the total RNA extracts from mice treated with saline or NV1066. It was run in triplicate on a thermal cycler (ABI Prism 7700; Applied Biosystems, Foster City, CA) and contained cDNA, TaqMan Universal PCR mix (Applied Biosystems), and target-specific TaqMan dye-labeled primer/probe (Applied Biosystems). The primers used for quantitative RT-PCR were for the expression of the early HSV-1 gene *ICP6* and late gene *LAT*. Each sample was measured quantitatively by RT-PCR and standardized to an 18S ribosomal RNA (rRNA) control. Probes used for *ICP6* included: ATA GCC AAT CCA TGA CCC TGT ATG (forward), GGG TGG AGG CTG GGA GG (reverse), and CAC GGA GAA GGC GGA CGG GA (probe). Probes used for *LAT* exon included: CCC ACG TAC TCC AAG AAG GC (forward), AGA CCC AAG CAT AGA GAG CCA G (reverse), and CCC ACC CCG CCT GTG TTT TTG TG (probe). Standard curves were generated from serial dilutions. Reverse transcription–polymerase chain reaction was performed under the following conditions: stage 1, 50°C for 2 minutes; stage 2, 95°C for 10 minutes; stage 3 (35 cycles), 95°C for 15 seconds and 60°C for 1 minute; and stage 4, 25°C.

Statistical Analysis

Student's *t* tests or analysis of variance (ANOVA) between group were used for statistical analysis as appropriate. Mantle–Haenszel and Fisher exact tests were used for evaluating differences in toxicity between groups. Differences were considered significant at $P < .05$. All data are presented as mean ± SEM, unless indicated otherwise. All experiments were repeated in triplicate. Data from representative experiments are shown.

Results

NV1066 Infection Effectively Expresses eGFP in Cancer Cells

The ability of NV1066 to infect and express eGFP in DU145 and PC3 (prostate carcinoma), ACC3 (salivary adenoid cystic carcinoma), and MiaPaCa2 (pancreatic adenocarcinoma) cell lines was assessed *in vitro* by fluorescence microscopy (Figure 1). All cells surviving by day 6 showed nearly 100% eGFP expression following NV1066 infection at an MOI of 10 (ratio of viral PFU to cancer cells). Even at an MOI of 1, the MiaPaCa2 and ACC3 cells showed nearly complete eGFP expression by day 6. The four cell lines showed a similar pattern of eGFP expression following NV1066 infection.

NV1066 Infection Selectively Expresses eGFP in Cancer Cells But Not in Nerves

The effect of NV1066 on cancer cells in association with nerves was evaluated using an *in vitro* NI model. Mouse DRG were implanted and grown in Matrigel adjacent to a colony of cancer cell lines on a six-well plate. Approximately 7 days after implantation, the DRG axons made contact with the tumor colony, and NV1066 (5 × 10^7 PFU) was injected into the Matrigel at this site. Twenty-four hours later, selective eGFP expression by the cancer cells was detected using fluorescence microscopy. This expression continued up to 5 days after infection (Figure 2). High-resolution microscopic images showed that neither the neuronal cell bodies (ganglia) nor their axons expressed eGFP ($n = 4$). Neither axonal growth nor nerve morphology was affected by the virus.

Intraneural Injection of NV1066 Allows Detection of NI In Vivo

The safety of NV1066 injection into murine sciatic nerves was first assessed. The left sciatic nerves of nude athymic mice were injected with NV1066 or with wild-type HSV-1 (F′ strain) at 5 × 10^7 PFU. The right sciatic nerves were injected with saline and served as controls. Measures of nerve function were assessed daily. Mice treated with NV1066 had normal sciatic nerve function and showed no change in behavior relative to the controls for up to 30 days after treatment ($n = 6$). In comparison, all mice treated with the F′ strain showed complete sciatic nerve paralysis within 4 days after treatment ($n = 6$) and died or required euthanasia by day 7.

The ability of NV1066 to express eGFP selectively in nerves invaded by cancer cells *in vivo* was evaluated. Tumors were established in the sciatic nerves of nude mice bilaterally by direct injection of 3 × 10^5 pancreatic (MiaPaCa2), prostate (PC3 and DU145), or adenoid cystic carcinoma (ACC3) cells into the distal portion of the nerve. Seven days after the establishment of tumors, animals were treated by an intraneural injection of 5 × 10^7 viral PFU of NV1066 or saline into the left sciatic nerve. In another group of mice, NV1066 was injected into normal sciatic nerves devoid of tumor cells. Two days after viral infection, mice were anesthetized, their sciatic nerves

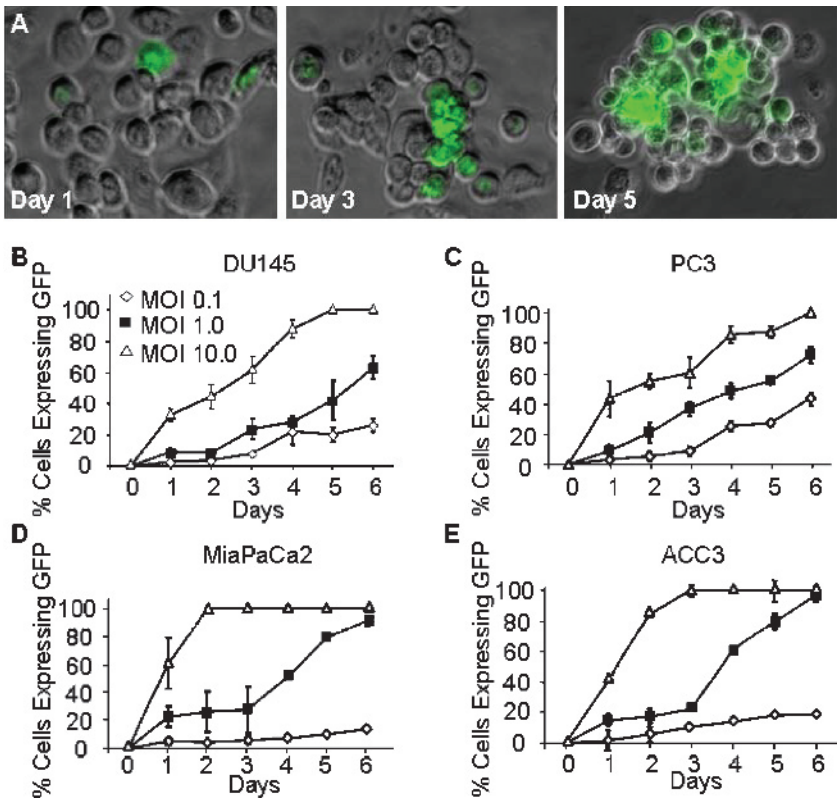

Figure 1. Infection with NV1066 induces expression of enhanced green fluorescent protein (eGFP) in neurotrophic human carcinoma cell lines *in vitro*. Human prostate carcinoma cells (PC3) were infected with NV1066 at a MOI of 1 for 5 days (A). Fluorescent microscopy imaging showed eGFP expression within 24 hours after infection. The number of cells expressing eGFP gradually increased within the next 6 days after infection (original magnification, ×100). The effect of various infection doses of NV1066 on eGFP expression by various neurotrophic cell lines. Human prostate carcinoma cell lines DU145 (B) and PC3 (C), pancreatic carcinoma cell line MiaPaCa2 (D), and salivary adenoid cystic carcinoma ACC3 (E). The cell lines were grown in culture for 6 days in the presence of various doses of NV1066.

exposed and inspected under a fluorescence dissecting stereoscope. A strong eGFP signal was detected selectively in nerves infiltrated by cancer cells and treated with NV1066 (Figure 3). There was no fluorescence in intraneural tumors treated with saline or in normal sciatic nerves devoid of cancer cells treated with NV1066 (n = 6). A strong fluorescent signal was recorded for each neurotrophic cell lines (Figure 4). Fluorescence microscopy and hematoxylin and eosin staining of nerve sections confirmed expression of eGFP selectively within the nerves infiltrated by cancer cells. No eGFP expression was detected by fluorescence microscopy in tumors treated with saline or in nerves without tumors treated with NV1066.

[^{18}F]-FEAU-PET Imaging with NV1066 Allows Detection of NI In Vivo

Previous reports have suggested that PET may be able to detect HSV replication *in vivo* in cancer cells using [^{18}F]-FEAU tracer as a substrate for HSV-1 thymidine kinase [11–13]. We explored the possibility of noninvasively imaging NI with PET following a single intraneural injection of NV1066. Bilateral sciatic nerve tumors (PC3 or ACC3) were treated with intraneural NV1066 injection (5×10^7 PFU) into the left nerve tumor, whereas the right sciatic nerve tumor of the same animal was injected with saline and served as control. Tumors treated with NV1066 had significantly higher levels of [^{18}F]-FEAU signal on the

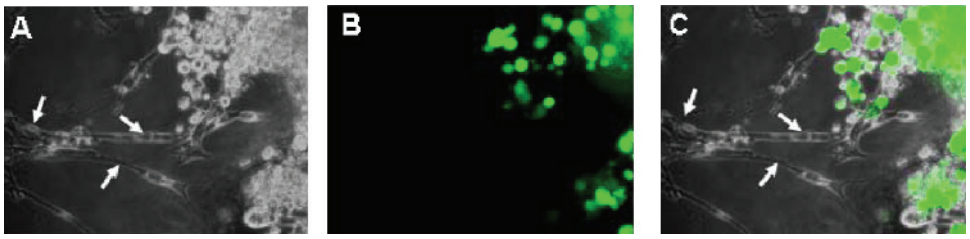

Figure 2. NV1066 selectively induces enhanced green fluorescent protein (eGFP) expression in cancer cells but not in nerves in an *in vitro* NI model. Dorsal root ganglia neurons were grown in Matrigel adjacent to a colony of cancer cells. NV1066 (5×10^7 PFU) was injected into the Matrigel 5 days after implantation. Microscopic images were acquired 48 hours after infection using bright field (A), fluorescence (B), and overlay (C) modes (original magnifications, ×40). High-magnification images illustrate that eGFP is expressed selectively by the cancer cells. Arrowheads indicate nerve cells. The virus had no visible toxic effects on the nerves.

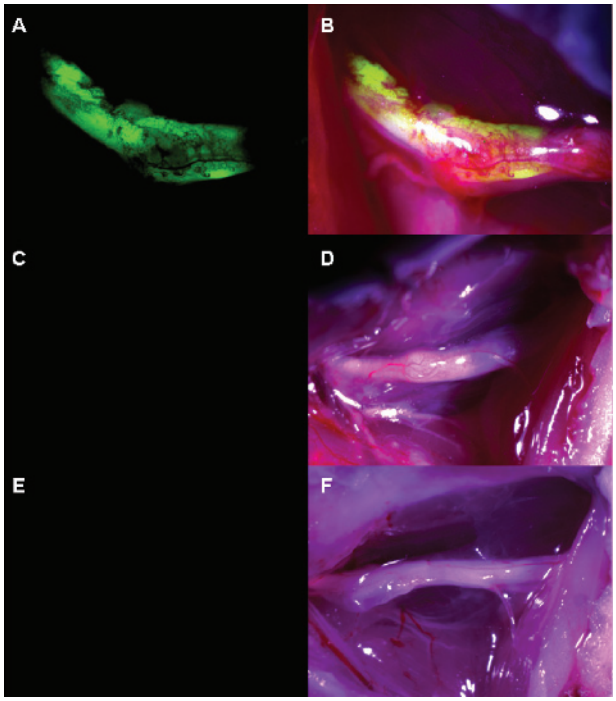

Figure 3. NV1066 selectively induces enhanced green fluorescent protein (eGFP) expression in nerves infiltrated by cancer in an *in vivo* NI model. Fluorescence image (A) and overlay image (B) showing eGFP expression in PC3 prostate cancer cells invading mouse sciatic nerves 48 hours after infection with NV1066 (5×10^7 PFU). Nerves invaded by cancer that were treated with saline had no fluorescence (C and D). Sciatic nerves without cancer invasion that were treated with a similar dose of NV1066 had no fluorescence (E and F).

PET scan than the contralateral tumors treated with saline (Figure 5, *A* and *B*). Normal tissues and normal nerves devoid of cancer cells injected with NV1066 showed PET signal similar to the background. After imaging, the specimens were excised and further analyzed with a gamma counter. Measurements of tissue radioactivity revealed a >3.6-fold increase of [^{18}F]-FEAU levels in the NV1066-treated nerves compared to controls (n = 2 per group).

Quantitative RT-PCR was performed on the RNA extracts from tumor specimens treated with NV1066 or saline. Primers for the HSV *ICP6* (early) and *LAT* (late) genes were used to assess viral infection. At 48 to 72 hours after viral injection, a significant increase in the relative number of *ICP6* and *LAT* mRNA transcripts was detected in sciatic nerves infiltrated by cancer cells but not in the brain or spinal cord of these mice (Figure 5*C*). No HSV mRNA transcripts were detected in sciatic nerves infiltrated by cancer cells and treated with saline.

Discussion

Surgical therapy for carcinomas with NI ideally requires resection of the tumor along with the involved nerves. In some cases, however, it may be difficult to determine whether a nerve is actually invaded by cancer, leaving surgeons with an intraoperative dilemma regarding whether to excise or preserve a nerve with an unclear status. Palpation and visual inspection of a nerve may not necessarily detect microscopic invasion. The preservation of an invaded nerve is likely to increase recurrence rates. Conversely, the resection of noninvaded nerves may inflict significant and unnecessary morbidity to patients. For prostate cancer, transection of the cavernous nerves causes erectile dysfunction and urinary incontinence [4]. For head and neck cancers, cranial nerve resection may cause blindness, facial nerve paralysis, facial numbness, hoarseness, dysphagia, dysarthria, and shoulder dysfunction [14,15]. The development of imaging methods for detecting NI may have clinical utility by assisting surgeons to determine whether nerve resection is required and to identify the portion of the nerve requiring resection. Furthermore, patients with NI often require adjuvant radiation therapy to reduce the risk of tumor recurrence [16]. A reliable noninvasive method for detecting NI could assist in targeting radiation therapy to areas where surgical resection is not feasible [17]. The appropriate preservation of noninvaded nerves, and treatment of nerves involved by cancer, may have a beneficial impact on both functional and oncologic outcomes [18,19].

We hypothesized that herpes oncolytic therapy may be appropriate for the clinical scenario of NI, as wild-type HSV-1 has a natural trophism for infecting peripheral nerves. Green fluorescent protein

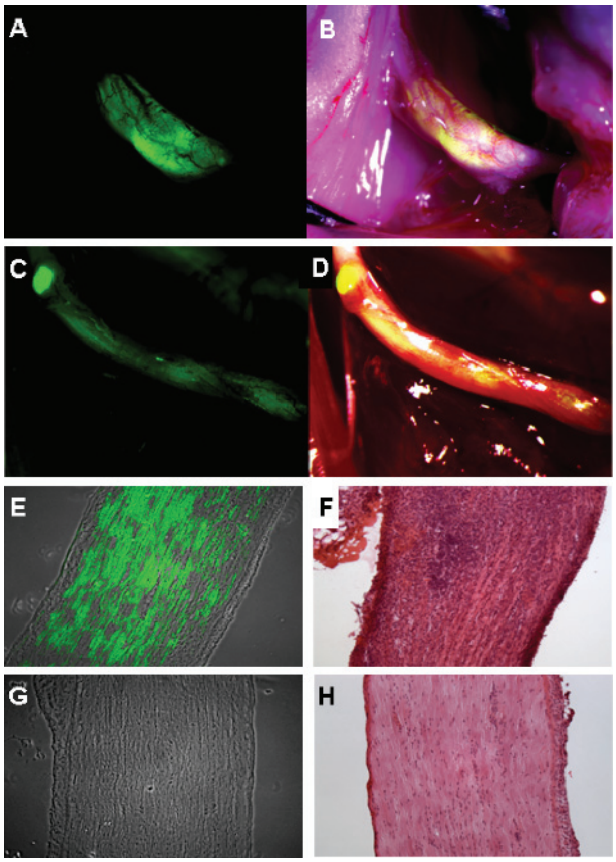

Figure 4. NV1066 selectively localizes areas of nerve infiltration by prostate and pancreatic carcinoma cells. Fluorescence image (A) and overlay image of prostate carcinoma (DU145)–derived tumor (B) and pancreatic carcinoma (MiaPaCa2)–derived tumor (C and D). Fluorescence microscopy (E) and corresponding hematoxylin and eosin image (F) of a sciatic nerve invaded by prostate carcinoma cells (PC3) and treated with NV1066. Fluorescence microscopy (G) and corresponding hematoxylin and eosin image (H) of a sciatic nerve without tumor treated with NV1066. Enhanced green fluorescent protein (eGFP) expression was found only in nerves infiltrated by cancer but not in normal nerves. Panels A to D are stereomicroscopic images. Panels E to H are microscopic images (original magnifications, ×10).

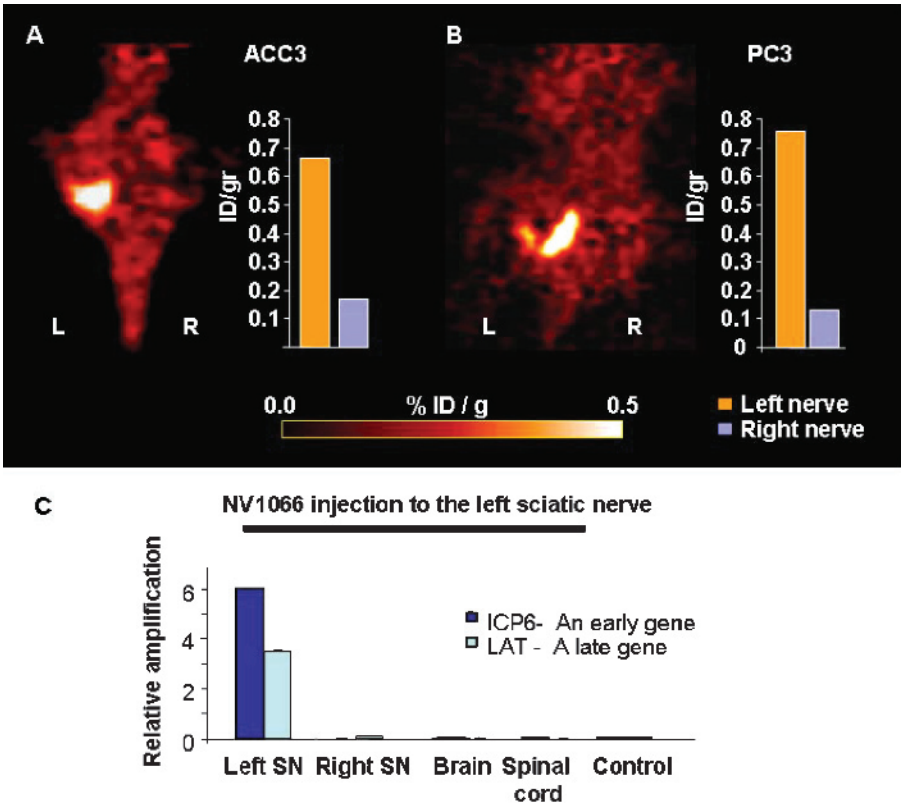

Figure 5. [^{18}F]-FEAU–PET imaging with NV1066 allows detection of cancerous NI *in vivo*. PET scanning of a mouse with bilateral ACC3 (A) or PC3 (B) tumors infiltrating the sciatic nerves. In each mouse, the left sciatic nerve was injected with NV1066 48 hours earlier, and the right nerve was injected with saline as a control. The NV1066-treated tumors had significantly higher uptake of [^{18}F]-FEAU (administrated by tail vein injection) on the PET scan. The bars on the right represent the accumulation of the radiotracer measured by a gamma counter in each nerve (orange – left nerve; blue – right nerve). The NV1066 treated nerves had a greater than 3.6-fold increase of radiotracer uptake than the right nerve. Normal tissue infected with NV1066 had no significant [^{18}F]-FEAU uptake. *R* indicates right side; *L*, – left side (C). RT-PCR performed at 72 hours after viral infection showing that early (*ICP6*) and late (*LAT*) viral mRNA were detected in sciatic nerves infiltrated by tumor cells, but not in the brain, spinal cord, or saline-treated nerves (controls).

has previously been used as marker for retrovirus and herpes vector gene transfer into various cancers including brain, mesothelioma, and breast tumors [20,21]. Similar vectors were also used as molecular imaging modalities to target radioactive tracers into cancers [12,22]. In this study, we demonstrate the utility of viral vectors to detect cancer cells invading nerves through noninvasive PET imaging and real-time fluorescence imaging. Using a genetically modified HSV-1, we demonstrate that a single injection of an attenuated, replication-competent vector can effectively express HSV-TK and eGFP in cancer cells invading nerves. All nerves infiltrated by tumors showed significant [^{18}F]-FEAU uptake capable of distinguishing between normal nerves and nerves infiltrated by cancer 48 hours after a single administration of NV1066. Intraoperatively, nerves infiltrated by tumor had significantly higher fluorescent signal compared with normal nerves. We also demonstrate that treatment with NV1066 had no adverse effect on nerve function and did not disseminate to the central nervous system. These findings suggest that NV1066 may safely be applied to effectively identify nerves infiltrated by cancer.

An implication of this study is that viral vectors might potentially be used as an imaging adjunct to guide the treatment of NI. Preoperative application of eGFP-expressing viruses could be performed before surgery through image-guided intraneural injections. For example, delivery could be performed through transrectal ultrasound-guided injections to cavernous nerve bundles in patients with prostate cancer [23]. Imaging of eGFP expression could then be visualized with fluorescent endoscopic imaging techniques [24]. Detection of small cancer foci with NV1066 appears highly sensitive, because all of the NV1066-treated cancers expressed HSV-TK or green fluorescent protein within 5 days. Furthermore, normal tissues failed to demonstrate background fluorescence. The sensitivity of this method to detect minimally invasive disease within nerves less than 0.5 mm in diameter is likely to be better than conventional imaging techniques (computed tomography, magnetic resonance imaging) that have resolutions able to detect gross tumor infiltration [25].

Nerve grafting may result in partial return of function in patients who require nerve resection due to cancer invasion. The only current means of assessing the length of tumor invasion along the nerve is nerve biopsy that requires resection of an additional nerve segment. Furthermore, because neurotrophic cancers may have skipped areas along invaded nerves, negative pathologic findings at the nerve margin does not guarantee complete cancer resection [26,27]. The proposed method in this study might allow the surgeon to visually delineate the extent of NI and to potentially detect varying sites of cancer longitudinally along nerves. Such an assessment may further assist adequate neural resection and facilitate decisions regarding graft reconstruction or adjuvant therapy [16].

None of the NV1066-treated animals suffered from clinically apparent side effects attributable to viral administration. The parent

virus from which NV1066 was derived, R7020, has a very favorable safety profile in *Aotus* owl monkeys, a primate exquisitely sensitive to herpes viral infections [28]. Even at a 10,000-fold higher dose than wild-type HSV-1, R7020 remained less toxic to *Aotus* monkeys as compared with HSV-1. A similar virus, NV1020, was recently studied in a phase I trial for patients with hepatic colorectal metastases. Doses of up to 1.3×10^9 PFU were administered by hepatic infusion pump without dose-limiting toxicity or significant adverse events attributable to the virus [29]. NV1020 has a highly favorable safety profile, a finding that has encouraged our investigation of its related vectors such as NV1066 for clinical application.

In conclusion, our study shows that an attenuated, replication-competent, herpes virus expressing eGFP can effectively and selectively detect NI by cancer cells both in preoperative and intraoperative setups. These findings hold significant clinical implications for potentially improving patient care by enabling (1) the detection of nerves infiltrated by cancer, (2) the selective preservation of normal nerves, (3) the potential delineation of the extent of neural infiltration, and (4) the guidance of adjuvant radiation therapy to areas not surgically accessible. This novel imaging approach might potentially improve the treatment of prostate, pancreatic, or head and neck cancers by preserving neural function and enhancing therapy of NI, potentially leading to reduced morbidity and improved oncologic outcomes.

Acknowledgments

We are grateful C. Moskaluk for providing the ACC3 cell line. Technical services provided by the MSKCC Small-Animal Imaging Core Facility are gratefully acknowledged. We also thank Meryl Greenberg for her editorial assistance.

References

[1] Byar DP and Mostofi FK (1972). Carcinoma of the prostate: prognostic evaluation of certain pathologic features in 208 radical prostatectomies. Examined by the step-section technique. *Cancer* **30**, 5–13.

[2] Conlon KC, Klimstra DS, and Brennan MF (1996). Long-term survival after curative resection for pancreatic ductal adenocarcinoma. Clinicopathologic analysis of 5-year survivors. *Ann Surg* **223**, 273–279.

[3] Kendirci M, Bejma J, and Hellstrom WJ (2006). Update on erectile dysfunction in prostate cancer patients. *Curr Opin Urol* **16**, 186–195.

[4] Tobisu K (2006). Function-preserving surgery for urologic cancer. *Int J Clin Oncol* **11**, 351–356.

[5] Singer PA, Tasch ES, Stocking C, Rubin S, Siegler M, and Weichselbaum R (1991). Sex or survival: trade-offs between quality and quantity of life. *J Clin Oncol* **9**, 328–334.

[6] Secin FP, Koppie TM, Scardino PT, Eastham JA, Patel M, Bianco FJ, Tal R, Mulhall J, Disa JJ, Cordeiro PG, et al. (2007). Bilateral cavernous nerve interposition grafting during radical retropubic prostatectomy: Memorial Sloan-Kettering Cancer Center experience. *J Urol* **177**, 664–668.

[7] Gil Z, Patel SG, Singh B, Cantu G, Fliss DM, Kowalski LP, Kraus DH, Snyderman C, Shah JP; International Collaborative Study Group (2007). Analysis of prognostic factors in 146 patients with anterior skull base sarcoma: an international collaborative study. *Cancer* **110**, 1033–1041.

[8] Nemzek WR, Hecht S, Gandour-Edwards R, Donald P, and McKennan K (1998). Perineural spread of head and neck tumors: how accurate is MR imaging? *AJNR Am J Neuroradiol* **19**, 701–706.

[9] Carew JF, Kooby DA, Halterman MW, Kim SH, Federoff HJ, and Fong Y (2001). A novel approach to cancer therapy using an oncolytic herpes virus to package amplicons containing cytokine genes. *Mol Ther* **4**, 250–256.

[10] Adusumilli PS, Eisenberg DP, Chun YS, Ryu KW, Ben-Porat L, Hendershott KJ, Chan MK, Huq R, Riedl CC, and Fong Y (2005). Virally directed fluorescent imaging improves diagnostic sensitivity in the detection of minimal residual disease after potentially curative cytoreductive surgery. *J Gastrointest Surg* **9**, 1138–1146; discussion 1146–1147.

[11] Serganova I, Doubrovin M, Vider J, Ponomarev V, Soghomonyan S, Beresten T, Ageyeva L, Serganov A, Cai S, Balatoni J, et al. (2004). Molecular imaging of temporal dynamics and spatial heterogeneity of hypoxia-inducible factor-1 signal transduction activity in tumors in living mice. *Cancer Res* **64**, 6101–6108.

[12] Bennett JJ, Tjuvajev J, Johnson P, Doubrovin M, Akhurst T, Malholtra S, Hackman T, Balatoni J, Finn R, Larson SM, et al. (2001). Positron emission tomography imaging for herpes virus infection: Implications for oncolytic viral treatments of cancer. *Nat Med* **7**, 859–863.

[13] Kuruppu D, Brownell AL, Zhu A, Yu M, Wang X, Kulu Y, Fuchs BC, Kawasaki H, and Tanabe KK (2007). Positron emission tomography of herpes simplex virus 1 oncolysis. *Cancer Res* **67**, 3295–3300.

[14] Mendenhall WM, Amdur RJ, Hinerman RW, Werning JW, Malyapa RS, Villaret DB, and Mendenhall NP (2007). Skin cancer of the head and neck with perineural invasion. *Am J Clin Oncol* **30**, 93–96.

[15] Terhaard C, Lubsen H, Tan B, Merkx T, van der Laan B, Baatenburg-de Jong R, Manni H, and Knegt P (2006). Facial nerve function in carcinoma of the parotid gland. *Eur J Cancer* **42**, 2744–2750.

[16] Han A and Ratner D (2007). What is the role of adjuvant radiotherapy in the treatment of cutaneous squamous cell carcinoma with perineural invasion? *Cancer* **109**, 1053–1059.

[17] Williams LS, Mancuso AA, and Mendenhall WM (2001). Perineural spread of cutaneous squamous and basal cell carcinoma: CT and MR detection and its impact on patient management and prognosis. *Int J Radiat Oncol Biol Phys* **49**, 1061–1069.

[18] Donatucci CF and Greenfield JM (2006). Recovery of sexual function after prostate cancer treatment. *Curr Opin Urol* **16**, 444–448.

[19] Garden AS, Weber RS, Ang KK, Morrison WH, Matre J, and Peters LJ (1994). Postoperative radiation therapy for malignant tumors of minor salivary glands. Outcome and patterns of failure. *Cancer* **73**, 2563–2569.

[20] Aboody-Guterman KS, Pechan PA, Rainov NG, Sena-Esteves M, Jacobs A, Snyder EY, Wild P, Schraner E, Tobler K, Breakefield XO, et al. (1997). Green fluorescent protein as a reporter for retrovirus and helper virus–free HSV-1 amplicon vector–mediated gene transfer into neural cells in culture and *in vivo*. *Neuroreport* **8**, 3801–3808.

[21] Eisenberg DP, Adusumilli PS, Hendershott KJ, Chung S, Yu Z, Chan MK, Hezel M, Wong RJ, and Fong Y (2006). Real time intraoperative detection of breast cancer axillary lymph node metastases using a green fluorescent protein–expressing herpes virus. *Ann Surg* **243**, 824–830; discussion 830–832.

[22] Koehne G, Doubrovin M, Doubrovina E, Zanzonico P, Gallardo HF, Ivanova A, Balatoni J, Teruya-Feldstein J, Heller G, May C, et al. (2003). Serial *in vivo* imaging of the targeted migration of human HSV-TK–transduced antigen-specific lymphocytes. *Nat Biotechnol* **21**, 405–413.

[23] Kravchick S, Yoffe B, and Cytron S (2007). Modified perianal/pericapsular anesthesia for transrectal biopsy of prostate in patients with anal rectal problems. *Urology* **69**, 139–141.

[24] Stummer W, Pichlmeier U, Meinel T, Wiestler OD, Zanella F, and Reulen HJ (2006). Fluorescence-guided surgery with 5-aminolevulinic acid for resection of malignant glioma: a randomised controlled multicentre phase III trial. *Lancet Oncol* **7**, 392–401.

[25] Galloway TJ, Morris CG, Mancuso AA, Amdur RJ, and Mendenhall WM (2005). Impact of radiographic findings on prognosis for skin carcinoma with clinical perineural invasion. *Cancer* **103**, 1254–1257.

[26] Nakao A, Ichihara T, Nonami T, Harada A, Koshikawa T, Nakashima N, Nagura H, and Takagi H (1989). Clinicohistopathologic and immunohistochemical studies of intrapancreatic development of carcinoma of the head of the pancreas. *Ann Surg* **209**, 181–187.

[27] Kumar PP, Patil AA, Ogren FP, Johansson SL, and Reeves MA (1993). Intracranial skip metastasis from parotid and facial skin tumors: mechanism, diagnosis, and treatment. *J Natl Med Assoc* **85**, 369–374.

[28] Meignier B, Martin B, Whitley RJ, and Roizman B (1990). *In vivo* behavior of genetically engineered herpes simplex viruses R7017 and R7020: II. Studies in immunocompetent and immunosuppressed owl monkeys (*Aotus trivirgatus*). *J Infect Dis* **162**, 313–321.

[29] Kemeny N, Brown K, Covey A, Kim T, Bhargava A, Brody L, Guilfoyle B, Haag NP, Karrasch M, Glasschroeder B, et al. (2006). Phase I, open-label, dose-escalating study of a genetically engineered herpes simplex virus, NV1020, in subjects with metastatic colorectal carcinoma to the liver. *Hum Gene Ther* **17**, 1214–1224.